PRELIMINARY DESIGN OF A REVOLUTE TO PRISMATIC MORPHING COMPLIANT JOINT

Nicolas Mouazé[1], Lionel Birglen[1]
[1]*Robotics Laboratory, Department of Mechanical Engineering, Polytechnique Montréal, Montréal, QC, Canada*
Email: nicolas.mouaze@polymtl.ca; lionel.birglen@polymtl.ca

ABSTRACT

The reduction of weight and size of mechanisms are important and difficult challenges considering portability, energy efficiency, and simplicity of fabrication. One of the solutions to address these issues consists of mechanisms with variable topology for which the mobility of the output is a succession of several simpler elementary motions. This change of mobility allows for achieving complex motions without necessitating a complicated design where many actuators or types of mechanical transmissions are required. Indeed, these variable topology mechanisms, also referred to as morphing mechanisms, have the ability to change their output motion throughout their workspace. For instance, as presented here, they can transition from a rotating to a translating output with a continuous and smooth travel of the actuation. Hand tools, medical devices and aerospace robotic end-effectors are potential applications of this technology. In this paper, the conceptual design of such a revolute to prismatic morphing joint and its implementation using compliant hinges are proposed. Additionally, performance indexes pertaining to the desired output motion are proposed. First, a pseudo-rigid body model of a design candidate is presented and simulations of this model are compared with finite element analyses to ensure accuracy. Then, several design features are quantitatively evaluated in order to propose improvements for future versions of the design.

Keywords: compliant mechanism, variable topology, pseudo-rigid model, finite elements.

CONCEPTION PRÉLIMINAIRE D'UNE ARTICULATION ROTOIDE COMPLIANTE CHANGEANT EN UNE LIAISON PRISMATIQUE

RÉSUMÉ

La réduction de l'encombrement et du poids des mécanismes sont des problèmatiques majeures et difficiles en tenant compte des questions de portabilité, de minimisation de la consommation d'énergie et de facilité de fabrication. Une des solutions apportées pour répondre à ces problèmes consiste à utiliser des mécanismes à topologie variable. La mobilité en sortie de ces mécanismes est une succession de plusieurs mouvements élémentaires simples. Cette caractéristique permet d'accomplir des mouvements complexes sans avoir besoin d'une architecture compliquée avec plusieurs actionneurs ou mécanismes de transmission. En effet, ces mécanismes à topologie variable ont la capacité de changer leur mouvement de sortie au sein de leur espace de travail, par exemple et comme présenté dans cet article, en passant d'une rotation à une translation de la sortie tout en gardant un actionnement continu et régulier. Dans cet article, un concept préliminaire de mécanisme passant d'une articulation rotoïde à une articulation prismatique, ainsi que sa réalisation avec des liaisons compliantes sont proposés. De plus, des indices de performance relatifs à la capacité de réaliser le mouvement désiré en sortie sont présentés. En premier lieu, un modèle pseudo-rigide du design est présenté et des simulations de celui-ci sont comparées avec des analyses par éléments finis afin de s'assurer de la validité du modèle. Plusieurs élements additionnels au design sont évalués ensuite quantitativement afin de proposer des améliorations pour de futurs versions du mécanisme.

Mots-clés : mécanisme compliant, topologie variable, modèle pseudo-rigide, éléments finis.

1. INTRODUCTION

Mechanisms with variable topology (MVT) have the ability to change their mobility during operation by switching their topologies [1]. These switches or variations occur through modifications of the number, type and/or configuration of their joints. This explains why they are sometimes referred to as *reconfigurable* mechanisms with variable joints in contrast to invariant topological structures. They are also referred to as morphing systems by biomimetism inspiration [2]. Similarly, morphing wings can be designed that change their aerodynamic properties, e.g. in [3], although in that case focus is often mainly placed on material properties rather than topologies. One of the main interests of MVT is to be able to achieve complex and shifting motions with the simplest mechanical structure possible. Indeed, motions usually realized by several mechanisms can be achieved with a single MVT solution. Similarly to underactuated mechanisms, MVT have the advantage of decreasing the number of actuators required for complicated tasks [4]. Cost, weight and size are thereby reduced and thus, MVT are a promising way to design mechanisms in particular in medical or aerospace fields where footprints and payloads are significant issues. In [5] a leg mechanism is shown that switches from one topology, which is advantageous when crossing an obstacle, to another stabler and faster when there is no obstacle, a feature closely related to the design presented in [6, 7]. Another example is the adjustable plier with a Revolute (R) to Prismatic (P) variable joint presented in [8]. Finally, in [9] a 3-URU parallel manipulator was shown to have multi-operational mode throughout its workspace, e.g. spatial translations, orientational wrist, planar motion.

MVT are mostly created with two topologies states [10] and can transition from one to the other. A simple and typical example is a four-bar linkage switching from an RRRR mechanisms to an RRRP [11–13] structure as illustrated in Fig. 1. As can be seen in this figure, one of the revolute joints can morph into a prismatic joint with a continuous motion at the input and it allows for a smooth transition between a rotation and a translation of the output link. This morphing joint is also called a variable kinematic joint. From the MVT classification proposed in [14] the mechanism illustrated in the previous figure is a type-II MVT because the variable topology is only due to a variation of the joint geometry. A direct switching between both configurations is an ideal case, but in practice there is always a transition and the latter poses a major design challenge. The variable joint morphs from a one degree-of-freedom (DOF) topology to a combination of two topologies with one DOF each in the transitional position. From this state, the system could finally become a RRRR or a RRRP mechanism without preference posing a potential issue as to how to control the motion. Other morphing techniques are presented in [2] while in [15] planar five-bar mechanisms are presented. Spatial systems with variable joints also exist, see for instance [16, 17].

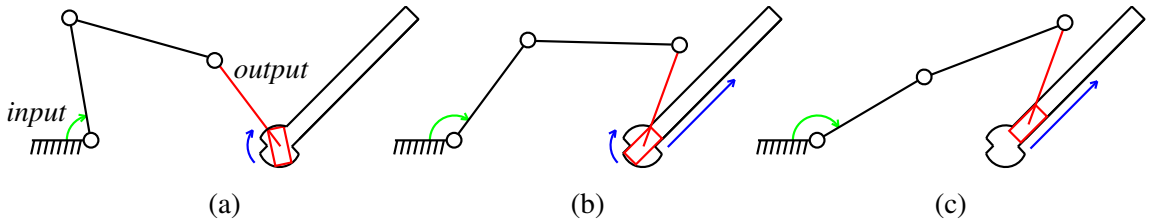

Fig. 1. Motions of a RRRR/RRRP morphing mechanism: a) RRRR topology phase, b) transition between topologies and c) RRRP phase.

To simplify manufacturing and assembly of linkages, mechanisms can be built relying on structural deformation to approximate lower-pair kinematic pairs. This technique is commonly referred to as compliant mechanism design [18, 19]. Two main approaches to design and build a compliant mechanism can be high-

lighted based on the literature. First, designs with flexure hinges where a localized thinning of the material is used to approximate revolute joints. Since the resulting deformation of the mechanisms is mainly concentrated in these thinned out parts of the mechanism, this is designated as localized compliance. Conversely, relying on distributed compliance is a second approach used when the mobility is created with an elongated section [20]. The latter technique allows typically for a wider range of motion because the stress undergone by the material due to the deformation is distributed to a greater volume of material. However, its accurate modeling is more challenging than with localized compliance. Both of these approaches are well known solutions to create compliant linkages [21]. To model the motions of compliant mechanisms using classical machine theory with added lumped compliances, Pseudo-Rigid Body Models (PRBMs) have been developed and make it easier to simulate and optimize compliant designs. Compliant revolute joints for instance can be very accurately modeled using PRBM and are most commonly found in practice. Prismatic joints on the other hand do not yet have a simple compliant equivalent although a series of thin parallel beams is often used in Micro-Electro-Mechanical Systems (MEMS) to constrain a seismic mass to a linear path [22, 23]. In [24] for example, a bistable micromechanism is introduced where a block of material is guided with two pairs of parallel thin beams of material that allow for that block to translate only.

While underactuated compliant mechanisms are widespread for grasping applications [25–27], to the best of the authors' knowledge there is no report of a compliant MVT design in the literature. The purpose of this paper is to present a proposition for the latter with a morphing compliant linkage transitioning from a revolute to a prismatic output motion while minimizing the intermediate phase. First, a general design is proposed in Section 2 followed by the introduction of performance indexes in Section 3. Then, results obtained with a numerical model are compared to dynamic simulations of that model (using MSC ADAMS) and also to results from a finite element analysis software (ANSYS) in Section 4. Finally, improvements of the design are proposed and their performances are evaluated in Section 5.

2. MODELLING

The conceptual design proposed in this work is presented in Fig. 2. The output is the motion at the right part of the mechanism (in red). The left part is assumed to be fixed to the ground. This mechanism is a compliant implementation of the linkage illustrated in the previous section. Between the ground link at the left and the output at the right, there are two kinematic chains. The first (upper) one is constituted by a thin beam (in green) shaped as a "V" and the lower one (in blue) includes two living flexural hinges. The objective is that the right output part of the mechanism, when actuated by a force at the point P, has first an almost pure rotational motion and then, switches to a linear translation. It is expected that during the first part of this motion, movement of the output is mostly due to the flexibility of the thin beam and the right flexural hinge, the former spreading out as the input force is not of sufficient magnitude yet to bend the left flexural hinge. Then, when the thin beam is completely unfolded and stretched, this beam and the bottom link act as two guides to create the linear motion again similarly to the linkage presented in Section 1.

Figure 3 illustrates the pseudo-rigid body model (PRBM) of the proposed compliant design at rest as well as the two ideal motions to reach when actuated. From the initial state (in Fig. 3(a)), when the mechanism is actuated by a force as illustrated in Fig. 3(b), the output of the MVT (namely the link from A_2 to A_5) is rotating around a fixed point. Then, as the force is increasing the trajectory of the output changes from a circular to a linear path (Fig. 3(c)). In each of these phases a virtual four-bar linkage can be used to approximate the motion of the mechanism. The transition between both phases is controlled by the stiffnesses of the lumped springs and the geometry of the design. In the first phase, A_2 is almost fixed since the stiffness K_1 is sufficient to prevent the rotation around A_1 due to the actuation force. Links from A_1 to A_2 and from

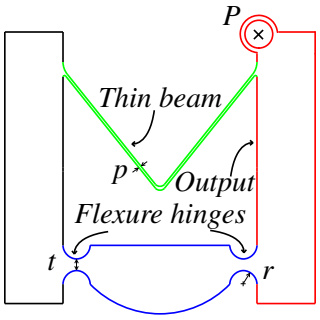

Fig. 2. Conceptual design of a morphing compliant R→P mechanism.

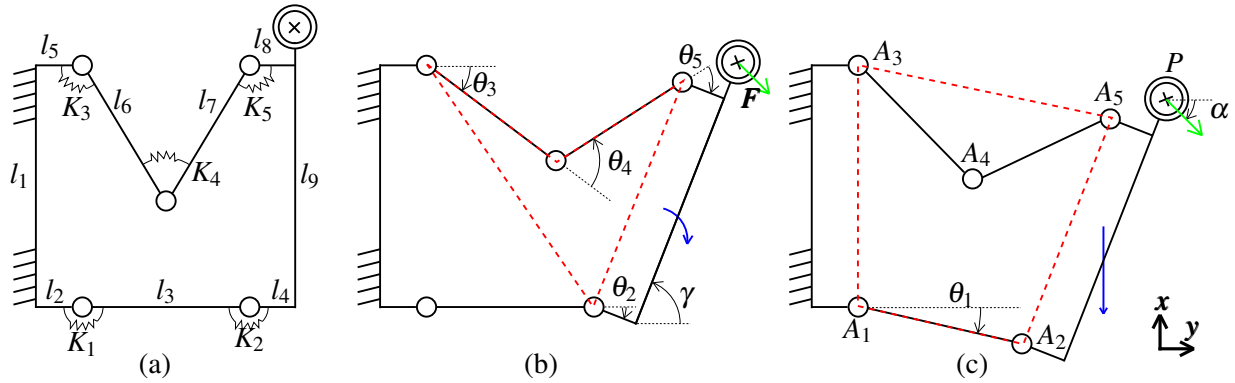

Fig. 3. PRBM of the MVT a) at rest, and desired motion during b) the rotation and c) the translation phase.

A_1 to A_3 are thus motionless. The vertices of the equivalent four-bar linkage in that phase are A_2, A_3, A_4 and A_5 as illustrated in dashed red lines in Fig. 3(b). Then, as the actuation force needed for a rotation around A_4 increases, the distance between A_3 and A_5 remains almost constant, which then defines the vertices of the second equivalent four-bar linkage for the translation phase, namely: A_1, A_2, A_5 and A_3. The last case is equivalent to designs with two pairs of parallel beams as in [28]. In the following, A_1 is assumed to be the origin of the coordinate system and the force has a constant orientation of $\alpha = -45°$ with respect to the $\boldsymbol{x}$-axis. This angle value is chosen in order for that force to be in the direction of first the rotation and then, the translation. The magnitude of the input force is assumed to be continuously incremented.

Positions and orientations of the output can be calculated from the parameters of the model and the input force increment by using the virtual work principle. To follow this approach, variations of the elastic potential energy stored in each of the springs modeling the compliant mechanism (with stiffness K_s with $s = 1,\ldots,5$ in the PRBM) is first calculated as:

$$\Delta E_{K_s,i} = \frac{K_s}{2}\Delta(\theta_{s,i} - \theta_{s,0})^2 \tag{1}$$

where the 0 and i subscripts indicate positions at the initial state and at the i^{th} increment of the actuation respectively. The stiffness K_s of the s^{th} spring is estimated with an approximated model from the literature [18, 19]. The thin beam is modelled as two flexible segments with forces and moments at their ends. Thus, the model with a combined force-moment end loading from [18] is used for this kinematic chain. It is worth mentioning that the accurate modelling of an initially curved compliant beam does not have a simple solution and the model chosen here is only a rough approximation.

Then, the virtual work of the actuation force $\boldsymbol{F}$ is:

$$\delta W_{F_i} = -F_i \delta \sqrt{(x_i - x_0)^2 + (y_i - y_0)^2} \cos(\boldsymbol{F}^T \boldsymbol{u}), \tag{2}$$

where F_i is the magnitude of the input force at the i^{th} increment, (x_i, y_i) the position of P the point of application of the force at the i^{th} increment and $\boldsymbol{u} = [x_i - x_{i-1}, y_i - y_{i-1}]^T$ the displacement vector between the position at the i^{th} and $(i-1)^{th}$ increments. At each step i and for each value of the input force F_i, the total value δW_i of the work from the actuation force δW_{F_i} and the variation of the potential energy of the internal springs is evaluated for several positions around the previous configuration. Then, the actual position of the mechanism corresponding to the minimum of W_i previously calculated is found, i.e.:

$$\delta W_i = \delta W_{F_i} + \sum_{s=1}^{5} \Delta E_{K_s,i}. \tag{3}$$

This allows to compute the values of the joint angles for each of the input force magnitude.

3. PERFORMANCE METRICS

The motion of the compliant MVT can be decomposed in three phases and thus, performance indices are also established according to this decomposition in order to evaluate the efficiency of the proposed design. In the first phase, the performance of the system can be measured according to the capability of the output to produce a pure rotation around a fixed point. This phase is assumed to take place between a zero input force $F_0 = 0$ at rest and a threshold magnitude F_a at the a^{th} increment. Thus, based on a proposed set of design parameters (geometry and material), the first step is to search for the best coordinates (X_0, Y_0) of the center of rotation of the output link and the distance R between this point and point P of the linkage. These parameters are found with the simplex search method implemented in MATLAB to establish the best circle segment that fits the path of the evaluated design in the selected range of force. Then, μ_1 the first performance metric can be computed as:

$$\mu_1 = \sum_{i=1}^{a} \left(\sqrt{(\boldsymbol{r}_{P_i}^T \boldsymbol{x} - X_0)^2 + (\boldsymbol{r}_{P_i}^T \boldsymbol{y} - Y_0)^2} - R \right)^2 \tag{4}$$

where $\boldsymbol{r}_{P_i}$ is the position of the point P relative to the origin A_1 for the input force magnitude F_i. The previous index evaluates the discrepancy between the ideal calculated circle path and the real trajectory of a selected point of the output link, namely P in the previous equation. In an ideal rotational motion of the output link, all points of the latter will move on a circle around the same fixed point. Therefore, another performance metric to quantify the motion of the output link can be similarly defined characterizing how close to a circle around the same point with coordinates (X_0, Y_0) the point A_6, arbitrarily chosen as the middle of A_2 and A_5, is:

$$\mu_2 = \sum_{i=1}^{a} \left(\sqrt{(\boldsymbol{r}_{A_{6,F_i}}^T \boldsymbol{x} - X_0)^2 + (\boldsymbol{r}_{A_{6,F_i}}^T \boldsymbol{y} - Y_0)^2} - \sqrt{(\boldsymbol{r}_{A_{6,F_0}}^T \boldsymbol{x} - X_0)^2 + (\boldsymbol{r}_{A_{6,F_0}}^T \boldsymbol{y} - Y_0)^2} \right)^2 \tag{5}$$

where $\boldsymbol{r}_{A_{6,F_k}}$ is the position vector of point A_6 for the force magnitude F_i. Both of the latter two metrics are defined as sums of squared values to stay positive in all cases.

The second phase, between the input force magnitudes F_a and F_b $(b > a)$ is defined as the transition between the revolute and prismatic compliant joint behaviors. During this phase, the actual motion of the

output is a mix between a pure rotation and a pure translation. A perfect mechanism will have an infinitely small transition between both motions and thus, a simple metric to quantify this aspect is:

$$\mu_3 = F_b - F_a \tag{6}$$

which is ideally zero.

Finally, during the prismatic joint phase between F_b and F_c the force maximal magnitude ($c > b$), the output link should have a linear motion and thus, the variation of its orientation (γ indicated in Fig. 3) must be as close to zero as possible. Therefore, an appropriate performance metric for this phase is:

$$\mu_4 = \sum_{i=b}^{c} (\gamma_{F_i} - \gamma_{F_b})^2 \tag{7}$$

where γ_{F_i} is the value of γ for the magnitude F_i. Again, minimal values of this metric are ideal. All the previously defined performances indexes can be used to measure the performance of a particular design and also optimize the compliant mechanism in order to approach the desired motion as much as possible. However, it should be noticed that these metrics are not independent of the selected scale and have all different units (square length, force, and square rad).

4. VALIDATION

In Figs. 4 and 5, a simulation of the numerical model proposed in Section 2 is compared to results from commercial softwares: a dynamic package (MSC ADAMS) and a finite element solver (ANSYS). The simulated material properties are those of Delrin (Young's modulus $E = 3.1 \cdot 10^9 Pa$ and Poisson's ratio $\mu = 0.35$) and Tab. 1 lists the PRBM stiffnesses and geometric parameters used as illustrated in Figs. 2 and 3. The variable e is the overall thickness of the mechanism in the out-of-the-plane direction (**z**-axis). Fig. 6 illustrates six successive positions along the range of the motion of the MVT and the associated deformations as evaluated with the FEA software. In the numerical model, spring stiffnesses modeling the distributed flexural beam are assumed equal ($K_3 = K_4 = K_5$). In Fig. 4 the motion of P goes from the top ($F = 0$ N) and moves along the curve toward the lower part of the figure. To compare the evolution of the orientation and the transition between the revolute and prismatic behavior of the mechanism, the figure is annotated with the value of the force at different increment values. A circle centered at (X_0,Y_0) with a R radius (noted Ideal Circle Path) is added as well to illustrate the ideal revolute path at the beginning of the motion, where X_0, Y_0 and R are calculated as presented in Section 3. Numerical values obtained are $X_0 = 49.6mm$, $Y_0 = 2.6mm$ and $R = 124.6mm$.

Table 1. Parameters of the simulations presented in Figs. 4 and 5 (all lengths are in *mm*, stiffnesses in N/m).

l_1	l_2	l_3	l_4	l_5	l_6	l_7	l_8	l_9	r	t	p	e	K_1	K_2	K_3	K_4	K_5
95	7	86	7	3.75	68	68	3.7	95	7	6	1.25	1	51.2	51.2	0.2	0.2	0.2

One can see from these results that the simulations from the numerical model and the dynamic software are indeed close, validating the numerical simulation based on the virtual work principle. However, a marked

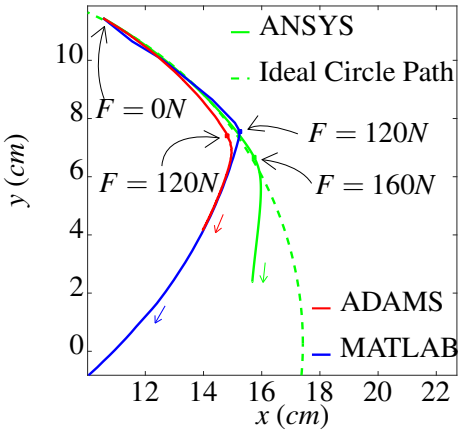

Fig. 4. Simulated motion of P.

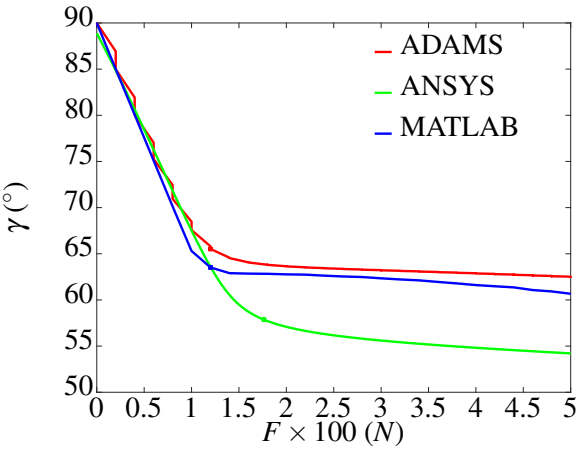

Fig. 5. Orientation of the output.

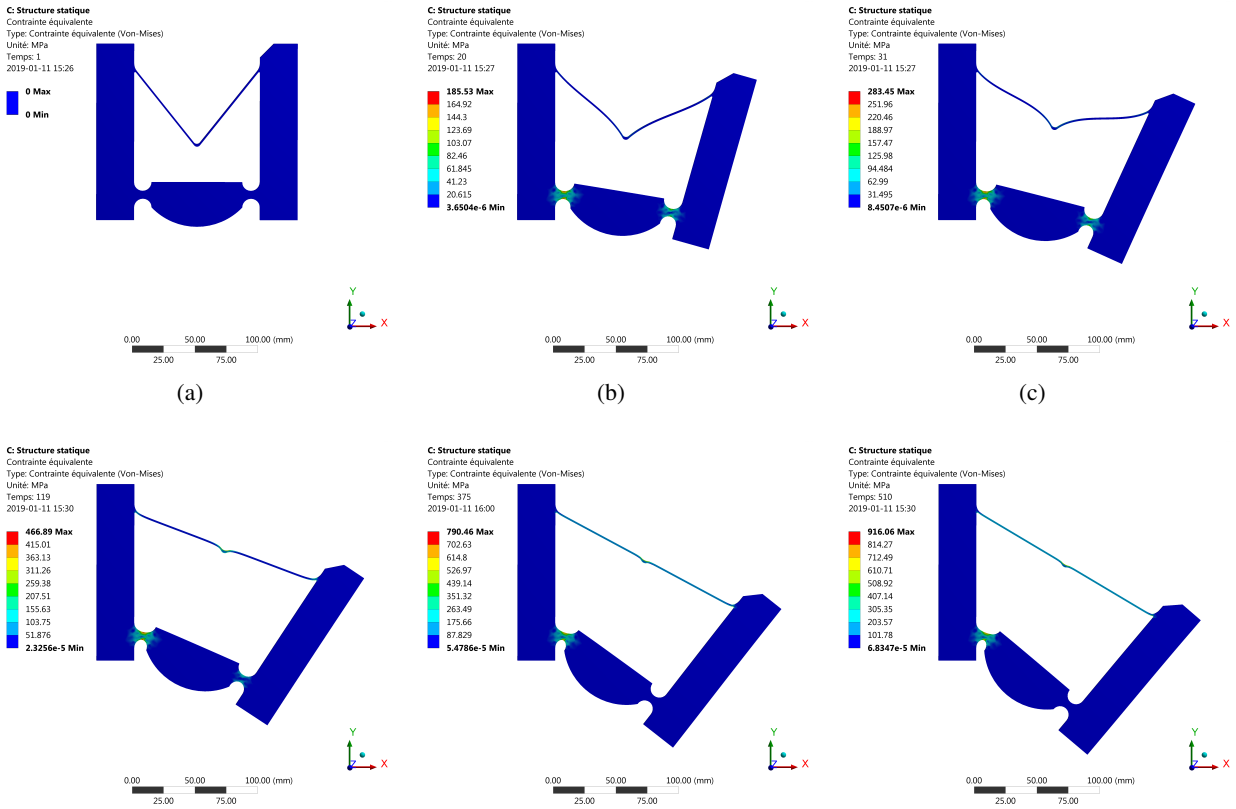

Fig. 6. Deformation of the MVT at (a) $F = 0N$, (b) $76N$, (c) $120N$, (d) $473N$, (e) $1500N$ and (f) $2000N$.

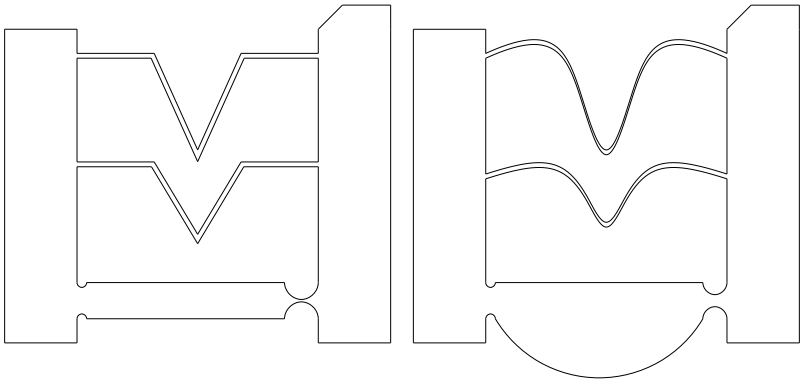

(a) Design #1 (D1) (b) Design #2 (D2)

Fig. 7. Conceptual designs.

discrepancy can be observed between these curves and the results from the FEA. The difference between these results may be explained by the approximated model of the compliant thin beam. Changing the value of the springs in the PRBM has little effect on the discrepancy which can therefore be traced mainly to the approximation of the geometry. The FEA and the model results in Fig. 5 show two parts with linear variations of the orientation of the output. The value of the force at the end of the first linear part is F_a while F_b is at the starting point of the second phase. These forces are selected by inspection of the plots. At the beginning, between $F = 0N$ and $F = 120N$ (see Figs. 6(a), 6(b) and 6(c)) the variations are important as expected for a rotational motion and then, between $F = 473N$ and $F = 2000N$ (see Figs. 6(d), 6(e) and 6(f)), these variations becomes quite negligible suggesting that indeed, the movement is close to a linear translation. Also the motion fits a segment of the ideal circle path, even though the radius of the latter is quite large. It should be noticed however that an important issue has been left unaddressed and is quite apparent from the values of the input force magnitudes: the deformations computed by the FEA indicate that the Von Mises stresses in the mechanism are actually higher than the yield limit of Delrin. This issue will be discussed in the next Section.

5. IMPROVEMENTS

Fig. 7 illustrates other potential design candidates for the MVT. Fig. 8 shows the motions of the point P (noted "Output") and Fig. 9 the orientations of the output link respectively for these new design candidates. In Fig. 8, ideal circular paths for each design are illustrated and noted "Circle". These circles are centered at the coordinates (X_0,Y_0) with a radius R whose values were found with the similar methodology as discussed before and used to calculate the performance metric μ_1, see Section 3. Table 2 presents the respective performance indexes. Variation of the orientation is constant at the beginning and at the end, thus transitions force values are computed from the orientation plots to calculate the associated indexes. The end of the revolute joint phase is observed at $F_a = 120N$, $32N$ and $128N$ for the initial design (ID), design 1 (D1), and 2 (D2) respectively. Then, the transitions end at $F_b = 473N$, $721N$ and $1030N$ for these same designs.

In design D1, two distributed compliance beams with identical geometry are used instead of a single one and the left flexure hinge was made stiffer in order to ensure that the bottom link starts to rotate only when the upper link is completely unfolded taking into account the results seen in Fig. 6(b). The performance indexes table illustrates that the initial design has the weakest performance during the revolute phase (large value of μ_2) and also the prismatic one (highest μ_4 but the difference is less significant than with μ_2). However, it is

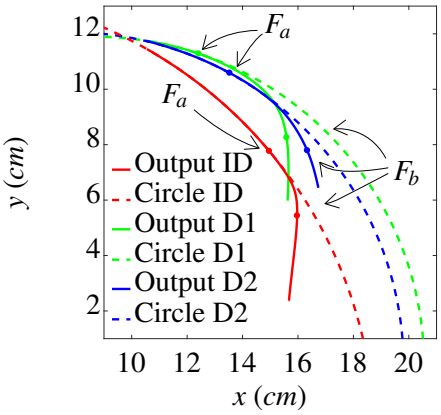

Fig. 8. Motion of the force contact point.

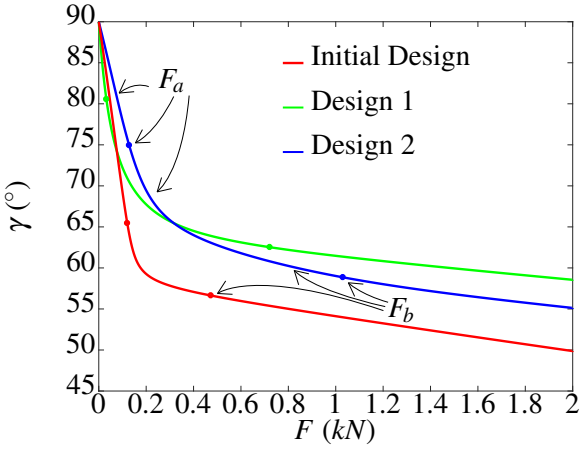

Fig. 9. Orientation of the output.

Table 2. Performance metrics of the designs presented in Fig. 7.

	Initial Design	Design 1	Design 2
μ_1	0.0026	0.0030	0.0285
μ_2	628	0.01	4
μ_3	353	689	901
μ_4	$5.4 \cdot 10^5$	$2.9 \cdot 10^5$	$2.8 \cdot 10^5$

the design with the smallest transition from one topology to the other and with the largest range of motion during the first phase. Finally, the second design D2 has a mix of several features and its geometry is adapted in order to maintain the Von Mises stress as low as possible. It presents good overall performances during the rotation and translation, but its transition phase is the longest. Other potential solutions to deal with excessive stresses during the operation of the linkage is to use another material with a larger range of elastic deformation such as rubber, or to use instead of a thin beam cut from the same block of material an insert with low compliance (a NiTinol sheet or even fabric wires for instance) added to that block of material. This would make manufacturing slightly more complicated but is a possible solution.

6. CONCLUSION

In this paper, the preliminary design of a compliant mechanism which is able to transition the motion of its output link from a rotation to a translation has been presented. This work constitutes a first step towards a more practical implementation and introduced a PRBM modeling the proposed system. This model was validated using a dynamical simulation package but the FEA results seem to point out that the selected PRBM is too coarse to accurately predict the required wide range of deformation. Performance metrics were then defined to help quantify how well the design candidate achieves its task and measure not only how accurately it can produce the desired output motions but also how "fast" it can transition from one to the other. Finally, design alternatives are proposed and compared to the initial iteration to highlight the compromise that seems to be required between the accuracy of the generated motion and the size of the transition phase.

ACKNOWLEDGMENTS

The support of the Natural Sciences and Engineering Research Council (Grant RGPIN327005) as well as the doctoral scholarship program of the Mechanical Engineering Department of Polytechnique Montreal are gratefully acknowledged.

REFERENCES

1. Kuo, C.H. and Yan, H.S. "On the mobility and configuration singularity of mechanisms with variable topologies." *Journal of Mechanical Design*, Vol. 129, No. 6, pp. 617–624, 2007.
2. Aimedee, F., Gogu, G., Dai, J., Bouzgarrou, C. and Bouton, N. "Systematization of morphing in reconfigurable mechanisms." *Mechanism and machine theory*, Vol. 96, pp. 215–224, 2016.
3. Sofla, A., Meguid, S., Tan, K. and Yeo, W. "Shape morphing of aircraft wing: Status and challenges." *Materials & Design*, Vol. 31, No. 3, pp. 1284–1292, 2010.
4. Birglen, L., Laliberté, T. and Gosselin, C.M. *Underactuated robotic hands*, Vol. 40. Springer, 2007.
5. Wu, J. and Yao, Y.a. "Design and analysis of a novel walking vehicle based on leg mechanism with variable topologies." *Mechanism and Machine Theory*, Vol. 128, pp. 663–681, 2018.
6. Fedorov, D. and Birglen, L. "Design of a self-adaptive robotic leg using a triggered compliant element." *IEEE Robotics and Automation Letters*, Vol. 2, No. 3, pp. 1444–1451, 2017.
7. Fedorov, D. and Birglen, L. "Geometric optimization of a self-adaptive robotic leg." *Transactions of the Canadian Society for Mechanical Engineering*, Vol. 42, No. 1, pp. 49–60, 2018.
8. Slaboch, B.J. and Voglewede, P.A. "Profile synthesis of planar rotational–translational variable joints." *Journal of Mechanisms and Robotics*, Vol. 6, No. 4, p. 041012, 2014.
9. Zlatanov, D., Bonev, I.A. and Gosselin, C.M. "Constraint singularities as c-space singularities." In "Advances in robot kinematics," pp. 183–192. Springer, 2002.
10. Kong, X., Gosselin, C.M. and Richard, P.L. "Type synthesis of parallel mechanisms with multiple operation modes." *Journal of Mechanical Design*, Vol. 129, No. 6, pp. 595–601, 2007.
11. Slaboch, B.J. and Voglewede, P.A. "Synthesis of a reconfigurable four-bar mechanism with variable joints." In "ASME 2014 International Design Engineering Technical Conferences and Computers and Information in Engineering Conference," pp. V05AT08A064–V05AT08A064. American Society of Mechanical Engineers, 2014.
12. Kuo, C.H. and Chang, L.Y. "Structure decomposition and homomorphism identification of planar variable topology mechanisms." *Journal of Mechanisms and Robotics*, Vol. 6, No. 2, p. 021002, 2014.
13. Slaboch, B.J. and Hobbs, B.W. "Novel classification of planar four-bar mechanisms with variable topology." In "ASME 2018 International Design Engineering Technical Conferences and Computers and Information in Engineering Conference," pp. V05BT07A006–V05BT07A006. American Society of Mechanical Engineers, 2018.
14. Shieh, W.B., Sun, F. and Chen, D.Z. "On the topological representation and compatibility of variable topology mechanisms." In "ASME 2009 International Design Engineering Technical Conferences and Computers and Information in Engineering Conference," pp. 1223–1230. American Society of Mechanical Engineers, 2009.
15. Balli, S.S. and Chand, S. "Synthesis of a five-bar mechanism of variable topology type with transmission angle control." *Journal of Mechanical Design*, Vol. 126, No. 1, pp. 128–134, 2004.
16. Wohlhart, K. "Kinematotropic linkages." In "Recent Advances in Robot Kinematics," pp. 359–368. Springer, 1996.
17. Yan, H.S. and Kuo, C.H. "Topological representations and characteristics of variable kinematic joints." *Journal of Mechanical Design*, Vol. 128, No. 2, pp. 384–391, 2006.
18. Howell, L.L. *Compliant mechanisms*. John Wiley & Sons, 2001.
19. Lobontiu, N. *Compliant mechanisms: design of flexure hinges*. CRC press, 2002.
20. Yin, L. and Ananthasuresh, G. "Design of distributed compliant mechanisms." *Mechanics based design of structures and machines*, Vol. 31, No. 2, pp. 151–179, 2003.
21. Jensen, B.D. and Howell, L.L. "Identification of compliant pseudo-rigid-body four-link mechanism configurations resulting in bistable behavior." *Journal of Mechanical Design*, Vol. 125, No. 4, pp. 701–708, 2003.
22. Cardou, P., Pasini, D. and Angeles, J. "Lumped elastodynamic model for mems: Formulation and validation." *Journal of Microelectromechanical Systems*, Vol. 17, No. 4, pp. 948–961, 2008.
23. Barel, M., Machekposhti, D.F., Herder, J., Tolou, N. and Sitti, M. "Permanent preloading by acceleration for

statically balancing mems devices." In "2018 International Conference on Reconfigurable Mechanisms and Robots (ReMAR)," pp. 1–11. IEEE, 2018.
24. Wilcox, D.L. and Howell, L.L. "Fully compliant tensural bistable micromechanisms (ftbm)." *Journal of Microelectromechanical Systems*, Vol. 14, No. 6, pp. 1223–1235, 2005.
25. Boudreault, E. and Gosselin, C.M. "Design of sub-centimetre underactuated compliant grippers." In "ASME 2006 International Design Engineering Technical Conferences and Computers and Information in Engineering Conference," pp. 119–127. American Society of Mechanical Engineers, 2006.
26. Doria, M. and Birglen, L. "Design of an underactuated compliant gripper for surgery using nitinol." *Journal of Medical Devices*, Vol. 3, No. 1, p. 011007, 2009.
27. Belzile, B. and Birglen, L. "A compliant self-adaptive gripper with proprioceptive haptic feedback." *Autonomous Robots*, Vol. 36, No. 1-2, pp. 79–91, 2014.
28. Machekposhti, D.F., Tolou, N. and Herder, J. "A review on compliant joints and rigid-body constant velocity universal joints toward the design of compliant homokinetic couplings." *Journal of Mechanical Design*, Vol. 137, No. 3, p. 032301, 2015.